Silver-assisted synthesis of gold nanorods: the relation between silver additive and iodide impurities

Sarah Jessl, Moritz Tebbe, Luca Guerrini, Andreas Fery, Ramon A. Alvarez-Puebla* and Nicolas Pazos-Perez**

S. Jessl, Dr. M. Tebbe, Prof. A. Fery, Dr. N. Pazos-Perez
Department of Physical Chemistry II, University of Bayreuth Universitaetsstrasse 30, Bayreuth 95440 (Germany).
E-mail: fery@ipfdd.de
Dr. L. Guerrini, Prof. R. A. Alvarez-Puebla, Dr. N. Pazos-Perez
Departamento de Quimica Fisica e Inorganica and EMaS, Universitat Rovira i Virgili Carrer de Marcel•lí Domingo s/n, 43007 Tarragona, Spain.
E-mail: ramon.alvarez@urv.cat; nicolas.pazos@urv.cat
Dr. L. Guerrini
Institute of Physical Chemistry, Hamburg University. Grindelallee 117, 20146 Hamburg, Germany
Prof. R. A. Alvarez-Puebla
ICREA, Passeig Lluís Companys 23, 08010 Barcelona, Spain.
S. Jessel
Current address: Institute for Manufacturing, Department of Engineering, University of Cambridge, 17 Charles Babbage Road, Cambridge CB3 0FS, United Kingdom.
Dr. M. Tebbe
Current address: Department of Chemistry, University of Toronto, 80 St. George Street, Toronto, Ontario M5S 3H6, Canada.
Prof. A. Fery
Current address: Institute for Physical Chemistry and Polymer Physics, Leibniz-Institut für Polymerforschung Dresden e.V., 01069 Dresden, Germany and Chair of Physical Chemistry of Polymeric Materials, Technical University Dresden, 01069 Dresden, Germany.

Keywords: gold nanorods, seed mediated growth, iodide and silver relation, plasmons, CTAB

Seed-mediated methods employing cetyltrimethylammonium bromide (CTAB), as a surfactant, and silver salts, as additives, are the most common synthetic strategies for high yield productions of quality Au NRs. However, the mechanism of these reactions is not yet fully understood and, importantly, significant lab-to-lab reproducibility issues still affect these protocols. In this study, we demonstrate the direct correlation between the hidden content of iodide impurities in CTAB reagents, which can drastically differ from different suppliers or batches, and the optimal concentration of silver required to maximize the nanorods yield. As a result, high-quality nanorods can then be obtained at different iodide contents. We interpret

these results base on the different concentrations of CTAB and CTAI complexes with Ag^+ and Au^+ metal ions in the growth solution, and their different binding affinity and reduction potential on distinct crystallographic planes. Notably, the exhaustive conversion of CTAI-Au^+ to CTAI-Ag^+ appears to be the key condition for maximizing the nanorod yield.

1. Introduction

Gold nanorods (Au NRs) are an interesting class of materials due to their unique size and shape dependent optical properties, with applications in electronics, optics, catalysis, diagnostics or therapy.[1-11] A wide variety of different synthetic protocols has been developed, including electro- and photo-chemical,[12-14] template assisted,[15-19] or seed-mediated methods.[20-23] Among all, those procedures based on wet chemistry are the most widely exploited due to their versatility, easiness, particle size and shape control, and upscaling possibilities.[20, 24-29]

Most metals like gold tend to crystallize in highly symmetric face-centered cubic lattices forming cubes and cuboctahedron structures which often became facetted spheres to minimize their surface energy at the nanoscale level.[30-31] Therefore, chemical additives are necessary to direct the asymmetric growth of nanoparticles while imparting colloidal stability.[25, 32-35] Seed-mediated methods employing cetyltrimethylammonium bromide (CTAB) as the surface-directing agent are the most common synthetic approaches for Au NRs.[20-21, 28, 36-38] Here, the use of preformed seeds results in improved mono-dispersity of the resulting particles, as the nucleation is separated from the asymmetric rod growth. Generally, the growth step is performed in the presence of CTAB, while gold seeds can be either prepared using citrate or CTAB as surface stabilizers. These two classes of seeds lead to Au NRs with very different crystallographic structures. Citrate-stabilized twinned seeds yield penta-twinned Au NRs with five {111} facets at both ends forming a pentagonal twinned prism and five {100} side facets that are arranged radially along the direction of elongation.[20, 27-28, 39-43] On the other hand, CTAB-capped seeds are single crystals,[21] and the asymmetric rod growth results in Au NRs

with {100} facets (two) at both ends and eight side surfaces, four {110} and four {100} facets, with no stacking faults or twins.[44] The synthesis of penta-twinned Au NRs does not require any additional additives but normally provides low yields (thus, additional purification steps might be needed). Contrary, in the case of single crystal seeds, the addition of $AgNO_3$ is required and allows for the efficient fabrication of Au NRs with yields up to 95%.[21, 30] Notably, improvements in the particle monodispersity and yield has been observed by addition of aromatic additives, such as phenol derivatives,[33, 38] or by using binary mixtures of different surfactants such as CTAB and sodium oleate (NaOL), or even bromide-free surfactants (like CTAC or trimethylstearylammonium chloride) in combination with NaOL.[45-46] Interestingly, bromide-free approaches can produce AuNRs even upon addition of NaI. However, as the iodide content was increased, Au NRs become more facetted (cuboid shape).

Small-angle neutron scattering (SANS) and small angle X-ray scattering (SAXS),[47] have revealed the formation of a CTAB bilayer on the Au NR, where the inner layer is bound to the gold surface by the quaternary ammonium head group.[48] This bilayer is positively charged and the cationic head groups are facing the aqueous medium at the nanoparticle-solvent interface.[49-50] Based on these results, the mechanism of Au NR growth was initially described as the reduction of micellized gold ions at the seed surfaces when brought in close proximity *via* collisions in solution. These collisions determine the reaction rate and are spatially controlled by the electrical double layer (EDL). Since the bilayer packing density is lower near the tip due to its curvature, the probability for micelles to approach the tips is higher compared to the sides. Thus, an interpretation based on the faster deposition of gold at the points of highest curvature leading to self-catalyzed rod formation was suggested.[51] However, this mechanism fails to explain both the initial change of seed morphology and the function of silver ions. Later, a major role in the Au NR synthesis was attributed to surface halide ions. In particular, it was suggested that bromide ions preferentially adsorb on low-

index gold surfaces,[52-53] therefore inducing an initial symmetry break followed by different growth rates of different crystallographic facets resulting in monodisperse rods.[54-57] While this mechanism addresses the initial symmetry breaking of the seeds, it still does not account for the key role of the $AgNO_3$ additive in the production of high-quality Au NRs. This lack of knowledge fueled a large number of basic studies aimed at bridging this gap. Nikoobakht et al.[21] suggested that AgBr is formed and adsorbed on the whole gold surface upon addition of $AgNO_3$, thus restricting the growth of Au NRs. On the other hand, Sau et al.[30] proposed that the AgBr adsorption occurs preferably on specific metallic regions which, in turn, directs the asymmetric growth and improves the rod yield. However, the implication of AgBr in the formation of Au NRs is not clear in the first place. In fact, it is known that halide anions form stable salts with Ag^+ (AgCl, AgBr, and AgI) having very low solubility constants (K_{sp}: 1.8×10^{-10}, 5.0×10^{-13}, 8.5×10^{-17} respectively) and, thus, they should be expected to preferably precipitate rather than adsorb onto the gold surface. To this point, the selective adsorption of AgBr on different gold facets was attributed to the presence of CTAB and the consequent formation of a complex between the surfactant and AgBr.[5, 21, 28, 30]

Currently, the most widely accepted mechanism relies on the underpotential deposition (UPD) of silver ions on the Au NR surface.[44] In this theory, a preferential deposition of a silver monolayer on the Au {110} facets is responsible for reducing the growth rate in those regions, therefore favoring the asymmetric gold growth in the [100] direction.[44] Other studies further confirmed the presence of about four monolayers of Ag on the final nanorods.[51, 58] This theory is also compatible with the formation of a AgBr-complex, which may be the reason for the lower reduction potential. However, while the selectivity of Ag^+ to be preferentially reduced on certain crystallographic planes of Au has been proven and is widely accepted within the scientific community,[59-61] the in-depth understanding of the mechanism is yet to be achieved and several key questions remain unanswered. In this regard, major reproducibility issues have been reported by many groups[52, 62-65] which have been mainly

related to inherent impurities present in CTAB,[62] and more specifically to the iodide content.[52, 64-66] In 2008, Korgel and co-workers[62] firstly revealed the remarkable importance of the CTAB source on the nanorod formation. The authors showed that spherical or rod particles are produced by using CTAB from different suppliers, and these different CTAB display slightly different binding strengths toward the seed particles, therefore influencing their growth rates during the growth step. At that time, they attributed the disruption of the nanorod formation in favor of spherical particles as the result of the presence of a very dilute impurity. Interestingly, in the same year, Millstone and co-workers[52] reported the unexpected presence of iodide on the surface of asymmetric gold nanoparticles produced with CTAB. In particular, they determined via inductively coupled plasma mass spectrometry (ICP-MS) the iodide content in several CTABs and investigated its impact on the fabrication of pentatwin Au NRs. While this approach is different from the silver-assisted method, it is noteworthy to highlight that particle morphologies have been observed to be highly dependent on the iodide content. Here, Au NRs yield increased with the iodide concentration until a certain threshold above which triangular and disk-like particles were preferentially obtained. The authors suggested that such dependence of nanoparticle morphology may be understood based on the preferential adsorption of iodide on the (111) crystal facets of Au.[52] On the other hand, Korgel and co-workers[63] reported that, when using the silver-assisted growth method, the presence of iodide as an impurity in the CTAB prevents the nanorod formation unless for very low iodide concentrations (i.e., for submonolayer coverage of the Au {111} surfaces). In this case, such nanorods can only be obtained with shorter aspect ratios. Similarly, Mirkin and co-workers[52] described that the concentration of iodide can be adjusted to selectively prepare either rods, prisms or spheres. Ha *et al.*[64] used penta-twinned seeds to prepare Au NRs adding different amounts of halide ions in the growth solution, and reported a progressive reshaping of rods to prisms as the iodide concentration was increased. On the other hand, DuChene *et. al.*[65] investigated the influence of different halides as surfactant counterions

(CTA-X; where X = Br, I, Cl) showing that, while bromide ions are essential for the Au NR formation, chloride and iodide inhibit their synthesis (spheres and prisms are preferentially formed, respectively). All these studies clearly demonstrate that halide ions are major factors in the synthesis of Au NRs, but they did not consider the role of Ag^+-ions since only penta-twined Au NRs (i.e., synthesis without addition of silver additive) were investigated. However, due to the high binding affinity between Ag and halide anions, it is reasonable to expect that their impact on the rod preparation using silver-assisted methods would be significantly intertwined. However, the interconnected role of Ag^+ and, especially, iodide ions has not been described so far, possibly because all previous works presented in the literature[5, 21, 28, 30, 44, 59] disregard a fundamental aspect: the inherent iodide concentration present as an impurity in CTAB.

Herein, we demonstrate that the concentration of iodide ions in CTAB is directly related to the amount of $AgNO_3$ required to optimize the synthesis of Au NRs. To do so, different batches of commercially available CTABs were acquired and their iodide content determined through ICP-MS. Notably, the iodide concentration not only proved to significantly vary from different suppliers, but also among batches provided by the same producer. As previously reported in the literature,[62] nanorod synthesis using identical synthetic protocol but different CTAB sources (i.e., different iodide contents) yielded very different sets of colloidal nanoparticles. Our results showed that by linearly adjusting the silver concentration with the iodide content, gold nanorods can be fabricated in good yields even for higher iodide content.[63] We suggest that the exhaustive conversion of CTAI-Au^+ to CTAI-Ag^+ is the first and major condition to be satisfied for improving the AuNRs yield, while the generation of CTAB-Ag^+ plays a secondary but still relevant role. On the other hand, we associate the presence of an excess of CTAI-Ag^+ content to (i) the reduction of the symmetry breaking efficiency for a progressively larger fraction of seeds at the early stage of the reaction and (ii) the subsequent depletion of the nanoparticle asymmetric growth. Our results provide new

major insights into the synthesis of AuNRs via the silver-assisted approach while providing valuable tools for optimizing the fabrication of these unique plasmonic materials.

2. Results and discussion

CTAB from various batches were acquired from two different suppliers and analyzed by inductively coupled plasma emission spectroscopy coupled with mass spectrometry (ICP-MS) to determine their iodide content. The results, summarized in **Table 1**, reveal an extremely large variability in iodide concentration (from 0.20 to 555 mg kg^{-1}).

Four separate syntheses of Au NRs were performed *via* a seed-mediated method as previously reported,[21] employing fixed amounts of single crystal seeds, $AgNO_3$ and CTAB in the growth solution but using different sources of the CTAB reagent (I^- content: 0.48, 1.0, 1.48, and 1.99 mg kg^{-1}). Each of the four syntheses was also repeated without adding silver salt. The extinction spectra of the resulting colloids (**Figure S1**) show marked differences. Overall, only gold nanoparticles prepared in the presence of silver ions displayed rod-like morphologies, but with large yield variability (from very poor to very good as seen in the different intensities of the longitudinal and transverse plasmon peaks shown in **Figure S1**) even though the same experimental conditions were applied to each colloidal synthesis. It is worth noting that this comparative study was performed using gold seeds prepared in the presence of the same CTAB reagent, corresponding to the one with the lowest iodide content (Merck, K93365042319, see **Table 1).** In this way, we removed the potential variability in Au NRs growth introduced by seeds with different crystallinity, while also minimizing the iodide introduced in the growth solution by the aliquot of seed particles. To test for the potential correlation between I^- content and optimum Ag^+ concentration, four distinct sets of Au NRs synthesis were carried out. For each set, a fixed amount of CTAB reagent (I^- content: 0.48, 1.0, 1.48, and 1.99 mg kg^{-1}) was used to prepare the growth solution while $AgNO_3$ concentration was varied over a broad range. The corresponding Au NR yield was estimated by calculating

the extinction ratio between the longitudinal and transverse plasmon peaks (I_L/I_T, referred along the manuscript as "intensity ratio"). The rationale for this approximation is that spheroidal (and some cubic) particles are mostly formed as by-products of the nanorod synthesis, providing plasmon resonances that largely overlap that of the transverse band from Au NRs.

Thus, large I_L/I_T ratios indicate a high Au NR yield with fewer spheroidal by-products contributing to the transverse mode. **Figure 1A-D** shows the extinction spectra of the different sets of colloids, while in **Figure 2A** the corresponding intensity ratios are plotted against the Ag^+ content. These results clearly indicate that the quality of Au NRs synthesis rapidly improves as the Ag^+ content is progressively incremented from zero until reaching an optimum concentration (corresponding to the intensity ratio maxima in **Figure 2A**, dots highlighted in yellow).

Interestingly, $AgNO_3$ concentrations exceeding the optimal threshold (see **Figure S2** for further details) result in yield reduction. In accordance with the previous discussion, the extinction spectra in **Figure 1** also show the emergence of a shoulder around 570 nm, corroborating that an excessive increase in $AgNO_3$ concentration leads to the formation of a larger fraction of by-products (spheres and cubes) in addition to the general nanorod growth.

The outcome of the optical characterization was further validated by TEM analysis of the obtained Au NRs (**Figure 3A** and **Figure S3**). Here, the percentages of rods, spheres, and cubes in each sample were estimated from several TEM images (at least 200 nanoparticles were evaluated for each analysis) and plotted in **Figure 3B**. Two common trends can be recognized: (i) the maximum relative content of Au NRs decreases for larger I^- concentrations. Specifically, for the case of CTAB with 0.483 mg kg^{-1} iodide, the Au NRs fraction peaked up to ca. 90% yield, while significantly lower values are reached for higher iodide concentration (75% and 70% for 1.48 and 1.99 mg kg^{-1} iodide, respectively); and (ii) the Au NR yield for a given iodide concentration increases when the Ag^+ content is raised up to a certain value, and

then progressively declines. These findings are fully consistent with the results extracted from the optical analysis of colloidal suspensions.

Extinction spectra in **Figure 1** also reveal a strong dependency of the longitudinal surface plasmon resonance peak position on both, the silver and iodide content. For all iodide concentrations, the plasmon band undergoes a marked red-shift as the silver amount is initially increased (**Figure 2B**) in good agreement with previously reported works.[21, 44, 67] However, for larger silver contents, a gradual blue-shift of the longitudinal SPR is observed in the case of Au NRs synthesized with the lowest iodide content. This shift to lower wavelengths becomes progressively less evident as the iodide content in the sample increases. On the other hand, at any given silver concentration, the data reveal a general trend of blue-shifting of the longitudinal SPR as the iodide content is increased.

Optimal $AgNO_3$ concentrations that provided maximum Au NR yields (**Figure 2A**, dots highlighted in yellow) and more red-shifted longitudinal SPR peak positions (**Figure 2B**, dots highlighted in green) are plotted in **Figure 2C** against the iodide content (here expressed both as mg kg^{-1} in the original CTAB reagent and as µM concentration in the growth solution). While maximum yield (yellow curve) shows a linear correlation between silver and iodide concentrations, the trend for longitudinal SPR peak position clearly diverges at higher iodide contents (green curve). This suggests that, in addition to the silver/iodide molar ratio, the absolute $Ag^+ + I^-$ content (for a fixed seed concentration) may also play an important role in determining the final morphological properties of Au NRs.

It is known that the longitudinal plasmon resonance of Au NRs shifts to higher wavelengths for increasing aspect ratios.[21, 44, 67] Thus, we also performed a TEM analysis of the morphological features of Au NRs to investigate the relation between the $AgNO_3$ concentration and changes in length (L), width (W) and aspect ratio (AR). Histograms of L, W and AR distributions of three classes of Au NRs (I^- content: 0.48, 1.48 and 1.99 mg kg^{-1}) obtained at four different silver concentrations are displayed in **Figure S4-S6**.

Overall, the collected data suggests an increase in AR upon increasing the $AgNO_3$ concentration (especially for 1.48 and 1.99 mg kg^{-1} iodide content) mainly due to an extension of the rod length (**Figure S7**). This agrees with what was previously reported in other studies.[21, 44, 67] On the other hand, for Au NRs prepared with low residual iodide content (0.48 mg kg^{-1}), the impact of the added amount of silver ions is limited and appears to qualitatively reproduce the trend observed for the longitudinal SPR peak position (i.e., a maximum of AR is achieved for an Ag^+ concentration around 0.06-0.08 mM, followed by a decrease for larger silver contents, **Figure S7**). As for the Au NR yield, the TEM analysis of the dried colloids largely corroborate the findings of the optical characterization in suspension, while minor numerical deviations can be ascribed to the different sample size (TEM analysis investigate a much smaller number of nanoparticles, deposited in random areas, as compared to the average that extinction spectra provide). In addition to alterations in L, W and AR, the examination of the TEM images also suggest that the rod tips become less round and start developing corners as the iodide concentration is increased (see representative images in **Figure S8**). Notably, a similar trend was also observed by Murray and coworkers[34, 46] when using combinations of CTAB-NaOL or in bromide-free synthetic approaches. This is not surprising since these approaches are also silver-assisted and, for the bromide-free case, it is expected that halides of higher electronegativity, as bromide and iodide, are also present as impurities.

The consistency of our findings was further tested over a much broader set of CTAB reagents at different iodide content. Specifically, 8 different CTABs (**Table 1**) and 6 mixtures of them (**Table S1**), were used to prepare growth solutions containing iodide concentrations ranging from 0.2 to 3.0 mg kg^{-1}. For each of the 14 iodide contents, a set of diverse syntheses were performed using different amounts of $AgNO_3$. Each of the Au NRs synthesis was repeated four times to assess reproducibility.

The resulting I_L/I_T intensity ratios are expressed as colors in **Figure 4**. For the sake of graphical clarity, the corresponding standard deviations were not reported in the figure, but they can be found in the supplementary information (**Figure S9-S11**), **Table 2** summarizes the data plotted in **Figure 4** showing the concentrations of Ag needed to achieve a higher yield of Au NRs. The illustrated data fully agree with our previous results, demonstrating that Au NRs can be fabricated for all tested CTABs by proportionally adjusting the amount of $AgNO_3$ to the iodide content. Nonetheless, as the iodide concentration becomes higher, the maximum achievable quality of the fabricated Au NRs diminishes. In fact, a maximum intensity ratio (up to 4.4, red dots in **Figure 4**) is obtained for iodide content in the 0.25-0.48 mg kg^{-1} range, while it significantly drops to 1.6 for iodide-rich CTABs (iodide concentration > 1.5 mg kg^{-1}). The diagram in **Figure 4** can then be used as a master graph for calculating the necessary $AgNO_3$ concentration required to produce Au NRs at high yields, for a given iodide content in the CTAB reagent (while CTAB concentration in the growth solution is fixed at 0.1 M).

As a final control experiment, we repeated the study by using NaI as a direct source of iodide, to rule out the potential role of other factors, such as unknown impurities present in the CTAB. To this end, different amounts of 1 mM NaI stock solution were added to a fixed volume of 0.1 M CTAB growth solution (with the lowest iodide content, 0.20 mg kg^{-1}) to obtain final iodide concentrations of 0.5, 1.0, 1.5 and 2.0 mg kg^{-1} (**Table S2**). The resulting Au NR yields, expressed in terms of intensity ratio, of Au NRs fabricated in the presence of different amounts of $AgNO_3$ are plotted in **Figure 5** and compared with those obtained using different types of CTABs. Here, we can clearly appreciate that it is indeed the absolute iodide content and not unidentified matrix effects that shapes the morphological features of Au NRs at different $AgNO_3$ concentrations.

These findings, in conjunction with those previously reported, lay the foundation for a more comprehensive interpretation of the silver-assisted growth mechanism of Au NRs. For the

sake of clarity, the crystallographic planes of Au NRs fabricated *via* the silver-assisted growth method are schematically visualized in **Figure S12**.

Previously, it has been indicated that halide ions preferentially adsorb on low-indexed gold surfaces (Au(111), Au(110) and Au(100)), with binding energies that scale with their polarizability ($I^->Br^->Cl^->>F^-$).[53] In particular, iodide ions appear to preferentially bind to the {111} and {110} facets, thus enabling a faster growth in the [100] direction.[52-53, 64] Similarly, halide anions display a very high affinity for Ag^+, again with binding affinities that decrease as $I^->Br^->Cl^-$.[53] On the other hand, it has been shown that, in the synthesis of Au NRs, the addition of silver ions slows down the growth rates on {110} facets, promoting the preferential deposition of Au° at the (100) planes (the most energy favorable locations).[44] Computational analysis of the binding energies of single Ag atoms on Au facets further corroborates the preferential silver deposition on {110} vs. {100}.[68-69] As reported in the introduction, the commonly accepted UPD theory suggests that silver is preferentially reduced on specific crystallographic planes[59-61] at a growth rate which is much smaller than gold. This is consistent with the minimal fraction of Ag° eventually retained at the Au NRs particles.[51, 58] Interestingly, molecular dynamics simulations also highlight the impact of the diverse geometric coordination of CTAB molecules at different Au faces in determining the accessibility of ions from the bulk solution to the gold surface.[70-72]

Taking all these considerations into account and combining it with our experimental results, we suggest the following mechanism (for the sake of clarity, **Figure 6 and Figure S13** offers a schematic sketch of the discussed concepts). The addition of Au salt to CTAB solution (with a fixed internal iodide content) leads to the formation of the CTAB-Au^+ complex[59, 61, 73] but also the corresponding CTAI-Au^+. These complexes display different crystallographic preferences, imparted by the diverse halide anion, but similar reduction potentials (i.e., similar growth rates on different facets). Upon addition of silver, and due to the higher affinity of halides for silver than for gold, CTAI-Ag^+ and CTAB-Ag^+ begin to form faster than their

corresponding Au complexes. This occurs to the detriment of CTAI-Au^+ complexes because the iodide amount is limited. As shown in **Figure 2C and Figure 4**, the optimum Ag^+ concentrations for maximum Au NR yield are directly determined by the initial amount of iodide in solution, and correspond to rather large Ag^+/I^- molar ratios (these values are approximately located within the 300 to 500 range). Overall, this suggests that the exhaustive conversion of CTAI-Au^+ to CTAI-Ag^+ is the first and major condition to be satisfied for improving the Au NR yield (**Figure 6A**). This can be explained in the following terms. While CTAI-Au^+ and CTAI-Ag^+ complexes retain similar preferential affinity for Au {110} facets imparted by the halide ion, the Ag^+ complex display a higher reduction potential.[53] Such a significant energy gap lays the foundation for the initial symmetry breaking of the seeds and their asymmetric growth in the [100] direction. This implies that the presence of CTAI-Au^+ restricts considerably the initial symmetry breaking and thus, the formation of Au NRs. Secondly, as it has been already reported,[59-61] the formation of CTAB-Ag^+ is also a key factor in the Au NR formation as shown by the excess of Ag^+ needed (compared to the I^- concentrations present in the CTABs) in order to achieve the maximum NR yield. The reason for that can be interpreted as follows. First, Ag^+ is consumed forming CTAI-Ag^+, therefore, suppressing the unfavorable formation of CTAI-Au^+. However, for very low I^- content, the effectiveness in slowing down the growth rates on {110} facets is not sufficient and more Ag^+ in the form of CTAB-Ag^+ is required to block these facets.

Notably, the drop in yield observed for Ag^+ concentrations beyond optimal values suggests that the extent of CTAB-Ag^+ formation also plays a relevant role in the final morphological features of the AuNRs, which is consistent with previous reports.[21] In particular, we attribute the negative impact on the quality of nanorods resulting from the generation of exceeding amounts of CTAB-Ag^+ to the competition between this complex and CTAB-Au^+ for binding to the (100) planes. This reduces the rate of asymmetric growth (**Figure 6A**), as clearly evidenced by the rapid loss in both yield and aspect ratio (**Figure 2A** and **2B**). Regardless, the

optimal Ag^+ concentration for a given iodide content appears to be the major factor providing the best compromise between the efficient conversion of CTAI-Au^+ to CTAI-Ag^+ and the generation of proper amounts of CTAB-Ag^+.

In addition to the Ag^+/I^- molar ratio, as previously pointed out, also the absolute iodide concentration in the growth solution affects the particle growth. As the iodide content augments, progressively higher silver concentrations are required to approach the optimum reaction conditions (as intuitively illustrated in **Figure 6A**). This simultaneously leads to an increase in molar ratios between iodide (and therefore the correspondingly tuned Ag^+ content) and seeds. Thus, a surplus of CTAI-Ag^+ adds up to the excess of CTAB-Ag^+ diminishing the degree of selective passivation via the unspecific deposition on other crystallographic planes (besides the (111) and (110)). Initially, this imposes a loss in symmetry breaking efficiency for a progressively larger fraction of seeds at the early stage of the particle growth, leading to a decrement of the maximum achievable Au NR yield (**Figure 2A** and **3B**). Secondly, an excess of CTAI-Ag^+ and CTAB-Ag^+ can also deteriorate the subsequent asymmetric growth of the forming nanorods, imposing a further reduction of the AR. This interpretation is consistent with the results reported in **Figure 2C**: under low iodide content (≤ 1.00 mg kg^{-1}), Au NR yield and AR are simultaneously optimized for the same silver concentration, while at higher iodide content (≥ 1.48 mg kg^{-1}) different silver concentrations are required to either maximize one or the other condition. In the first scenario, both conditions (yield and NR morphology) are mainly determined by the symmetry breaking efficiency. In the second scenario, the excess of I^- (and, thus, Ag^+) also starts influencing the final nanorod morphology in the successive growth process (**Figure 3A**), while Au NR yield is only affected by the initial symmetry breaking event.

These considerations also account for the impact of iodide and silver on the position of the longitudinal SPR. For a given iodide content, initial addition of Ag^+ results in the generation of longer nanorods with higher AR (**Figure S7**), leading to a red-shift of the plasmon band,

because of a more efficient passivation of the {111} and {110} surfaces promoted by the conversion of CTAI-Au^+ to CTAI-Ag^+. However, an increment of silver concentration beyond an optimal value simultaneously reduces the yield and facilitates the formation of thicker rods (blue-shift of the longitudinal plasmon band), as a consequence of an excess of CTAB-Ag^+ that worsen the rate of asymmetric growth. On the other hand, the absolute iodide content plays a major role in determining the tunability of the plasmon feature, blue-shifting the wavelength range as the iodide concentration is increased (**Figure 2B**). In this case, the presence of exceeding amounts of CTAI-Ag^+ induces the formation of thicker rods with a more pronounced rectangular shape (**Figure S8**).

Finally, as free-iodide CTAB reagents are not commercially available, it was not possible to investigate in detail the role of iodide content in the 0 to ca. 0.20 mg kg^{-1} range and, thus, univocally assess if the presence of a sufficiently small amount of iodide is actually advantageous for the efficient synthesis of Au NRs. Nonetheless, we do notice that the data illustrated in **Figure 4** show that a plateau in the intensity ratio is approached for iodide contents below ca. 0.4 mg kg^{-1}, which may suggest that a further decrease of iodide concentration in the unexplored 0-0.20 mg kg^{-1} range would not be beneficial for improving the rod yield. These concepts are schematically resumed in **Figure 6B**.

3. Conclusions

In summary, we have demonstrated the unique correlation between the content of iodide impurities in CTAB reagents and the optimal concentration of Ag^+ in the silver-assisted synthesis of Au NRs. The iodide content in different CTAB batches displays an extremely high variability, even for materials acquired from the same producer. The necessary amount of Ag^+ to be added in the growth solution, to maximize the Au NR yield, scales linearly with the iodide content (and correspond to rather large Ag^+/I^- molar ratios). However, increasing the iodide concentration above a certain threshold value, results in a decrease of the maximum

achievable Au NR yield. At the same time, the morphological features of the nanorods changed, showing a decrease of the aspect ratio as well as a transition of the tip geometry from round to cubic-like.

These experimental evidence were combined with the data reported in the literature, and we propose the following interpretation. The exhaustive conversion of CTAI-Au^+ to CTAI-Ag^+ is the key condition to be fulfilled to achieve a maximum in Au NR yield. CTAI-Ag^+ preferentially binds to Au {110} facets, as CTAI-Au^+, but exhibits a higher reduction potential, which promotes initial symmetry breaking of the seeds and their asymmetric growth in the [100] direction. However, exceeding amounts of silver ions diminish the quality of the Au NR synthesis (both in yield and aspect ratio), as a result of the generation of large fractions of CTAB-Ag^+ which compete with CTAB-Au^+ binding to the (100) planes. On the other hand, the absolute iodide concentration plays also a major role in defining the morphological features of the gold nanoparticles. When the iodide content surpasses a certain threshold (ca. 0.4-0.5 mg kg^{-1}, under our experimental conditions), a surplus of CTAI-Ag^+ is generated which reduces the degree of selective passivation for specific planes, therefore depleting the symmetry breaking efficiency of the seeds. For very large iodide contents, the excess of CTAI-Ag^+ also begins to extensively impoverish the second step of asymmetric growth of the Au NRs, leading to a further reduction of their aspect ratio.

Our results provide new major insights into the synthesis of Au NRs via the silver-assisted synthesis approach: (i) the direct correlation between the residual iodide content in CTAB reagent and the required amount of $AgNO_3$ additive to maximize the yield of Au NRs production has been revealed and described; and (ii) the dependence of the geometrical features of the particle (mainly, their tip extremities) from the absolute iodide (and, thus, silver) content has been elucidated. These results equip the scientific community with fundamental practical tools for a systematic and general protocol for the optimization of the silver-assisted growth method for the Au NRs production which can be potentially

implemented in every lab. Moreover, it is expected that the unveiling of the tight relation between the iodide content and silver concentration as a major synthetic parameter in the nanorod preparation can also play an important role in other seeded-growth syntheses using halide-containing reagents, therefore paving the way for further improvements of particle tunability and lab-to-lab reproducibility. In particular, we believe that these findings will significantly simplify the route to the efficient synthesis of Au NRs, in particular facilitating those non-highly-specialized researchers in dealing with the fabrication of these unique plasmonic materials.

4. Experimental Section

Materials and methods: Ascorbic acid (AA, 99.5 %) and Hydrochloric acid (HCl, 37 %) were acquired from Grüssing, Germany. Cetyltrimethyl ammonium bromide (CTAB, 99.8 %) was purchased from two suppliers (Sigma-Aldrich and Merck) and acquired from different batches (batch numbers: 091M0156V, K91921142 432, K93093842 050, K93211442 211, K93258242 225, K93365042 319, K93377642 325). Sodium chloride (NaCl, 99.98 %) was obtained from Fisher Scientific, Germany. Gold(III)chloride trihydrate ($HAuCl_4$, 99.9 %), silver nitrate ($AgNO_3$, 99.9999%), sodium iodide (NaI, 99.999 %), and sodium borohydride ($NaBH_4$, 99%) were bought from Sigma-Aldrich, Germany. All reactants were used without further purification. Milli-Q water (18 MΩ cm^{-1}) was used in all aqueous solutions. All the glassware was cleaned with aqua regia prior experiments.

Synthesis of gold nanorods: Gold nanorods of various aspect ratios were produced according to the previously reported seed-mediated procedure.[21] Briefly, seed particles were prepared by dissolving 0.18223 g CTAB in 4.7 mL of Milli-Q water thermostated at 32°C (0.1 M, CTAB). The solution was stirred at 700 rpm while an aliquot of a $HAuCl_4$ solution was added to yield a final $HAuCl_4$ concentration of 2.5×10^{-4} M. Upon $HAuCl_4$ addition, the color of the solution changed from transparent to yellow. Subsequently, freshly prepared $NaBH_4$ (300 μL,

0.01 M) was quickly injected meanwhile the solution was energetically stirred (1200 rpm). After addition, the color immediately changed from yellow to light brown which darkened after several minutes. Stirring was continued for 1h at open atmosphere to allow the $NaBH_4$ to decompose avoiding overpressure at 32°C to prevent CTAB crystallization.

Next, a growth solution was prepared by dissolving CTAB in Milli-Q water (f.c. 0.1 M, 100 mL). Subsequently, the solution was thermostated at 32°C. Followed by the addition of $HAuCl_4$ (f.c. 2.5×10^{-4} M) leading to an orange color of the solution. After that, ascorbic acid (0.1 M, 374 µL) was added to the solution. An immediate change from orange to transparent was observed. Hydrochloric acid (0.1 M, 650 µL) was used to lower the pH to 3-4. After each addition of the different reagents, the reaction vessel was vigorously shaken.

Next, the growth solution was divided into 10 mL aliquots and, to each of them, the calculated amount of $AgNO_3$ was added. The final $AgNO_3$ concentration ranged from 0.02 mM to 0.32 mM, depending on the experiment. Finally, 100 µL of the as-prepared seeds were carefully added to the foam of the growth solution. Then the mixture was vigorously shaken and the bottles were left undisturbed at 32°C for 24 h.

For TEM characterization of the Au NRs, the CTAB concentration was reduced from 0.1 M to approximately 0.001 M. This was done by centrifuging 1 mL of the as-prepared rods at 9000 rpm for 20 minutes. The supernatant was removed and the rods were redispersed with additional 900 µL Milli-Q water. The whole process was repeated twice but, in the last step, the centrifugation was performed at 7000 rpm, and no water was added to increase the concentration of Au NR in solution.

Iodide concentration studies: ICP-MS was used to determine the exact iodide concentration in each CTAB batch. Solutions of CTAB were prepared from batches with different internal iodide concentrations. Appropriate mixtures of CTAB solutions were prepared to tune the final iodide concentration. The exact iodide contents from the different CTAB batches and their mixtures are listed in **Table 1** and **Table S1** respectively. In a second study, different

amounts of a 1 mM sodium iodide (NaI) stock solution were added to a 0.1 M surfactant growth solution prepared using the CTAB batch with the lowest internal iodide concentration (0.203 mg/kg). After that, the growth solutions were used immediately, or after one-day incubation, following the same procedure as previously described. A summary of the detailed parameters is displayed **Table S2**.

Characterization: UV-VIS spectroscopy was recorded with a Specord 250 plus from Analytik Jena. Size and shape characterization of the nanoparticles was performed with transmission electron microscopy (TEM, Zeiss 902 operating at 80 kV).

Supporting Information

Further TEM images, histograms, measurements of width, length and aspect ratio. Plots showing the correlation between the width, length, aspect ratio and IR vs. AgNO3 for different amounts of iodide, tables showing the mixtures of different CTABs and the amounts of externally added NaI, and the schematic crystallographic structure of a Au NR.
Supporting Information is available from the Wiley Online Library or from the author.

Acknowledgements

This work was funded by the Spanish Ministerio de Economia y Competitividad (CTQ2014-59808R, CTQ2017-88648R, RYC2016-2033 and RYC2015-19107), the European Research Council (Marie Curie Actions FP72014-623527 and ERC-2012-StG 306686 (METAMECH)) and the Generalitat de Catalunya (2014-SGR-480). M.T. acknowledges funding in the framework of the Bavarian elite promotion act (BayEFG). S.J. and M.T. were supported by the Elite Network Bavaria within the framework of the Elite Study Program “Macromolecular Science”. This project has also received funding from the European Union Horizon 2020 research and innovation program under the Marie Skłodowska-Curie grant No 712.949 (TECNIOspring PLUS), as well as from the Agencia para la Competitividad de la Empresa de la Generalitat de Cataluña. Finally, we would like to thank C. Kunert for TEM measurements.

Conflicts of interest

There are no conflicts to declare.

References

[1] W. Jiang, Y. S. KimBetty, J. T. Rutka, C. W. ChanWarren, *Nat. Nanotech.* **2008**, *3*, 145-150.
[2] C. J. Murphy, A. M. Gole, J. W. Stone, P. N. Sisco, A. M. Alkilany, E. C. Goldsmith, S. C. Baxter, *Acc. Chem. Res* **2008**, *41*, 1721-1730.
[3] C. J. Orendorff, T. K. Sau, C. J. Murphy, *Small* **2006**, *2*, 636-639.
[4] L. M. Liz-Marzán, *Langmuir* **2006**, *22*, 32-41.
[5] K. Zhou, Y. Li, *Angew. Chem. Int. Edit.* **2012**, *51*, 602-613.
[6] A. J. Haes, D. A. Stuart, S. Nie, R. P. Van Duyne, *J. Fluoresc* **2004**, *14*, 355-367.

[7] J. Morla-Folch, L. Guerrini, N. Pazos-Perez, R. Arenal, R. A. Alvarez-Puebla, *ACS Photonics* **2014**, *1*, 1237-1244.
[8] M. Tebbe, P. Cherepanov, E. V. Skorb, S. K. Poznyak, J. G. de Abajo, A. Fery, D. V. Andreeva, R. A. A. Puebla, N. Pazos-Perez, *Part. Part. Syst. Char.* **2014**, *31*, 1134-1140.
[9] M. Tebbe, M. Maennel, A. Fery, N. Pazos-Perez, R. A. Alvarez-Puebla, *J. Phys. Chem. C* **2014**, *118*, 28095-28100.
[10] W. Chen, M. Tymchenko, P. Gopalan, X. Ye, Y. Wu, M. Zhang, C. B. Murray, A. Alu, C. R. Kagan, *Nano Lett.* **2015**, *15*, 5254-5260.
[11] A. Lee, A. Ahmed, D. P. dos Santos, N. Coombs, J. I. Park, R. Gordon, A. G. Brolo, E. Kumacheva, *J. Phys. Chem. C* **2012**, *116*, 5538-5545.
[12] Yu, S.-S. Chang, C.-L. Lee, C. R. C. Wang, *J. Phys. Chem. B* **1997**, *101*, 6661-6664.
[13] S.-S. Chang, C.-W. Shih, C.-D. Chen, W.-C. Lai, C. R. C. Wang, *Langmuir* **1999**, *15*, 701-709.
[14] F. Kim, J. H. Song, P. Yang, *J. Am. Chem. Soc.* **2002**, *124*, 14316-14317.
[15] M. P. Pileni, T. Gulik-Krzywicki, J. Tanori, A. Filankembo, J. C. Dedieu, *Langmuir* **1998**, *14*, 7359-7363.
[16] C. R. Martin, *Chem. Mater.* **1996**, *8*, 1739-1746.
[17] T. Kyotani, L.-f. Tsai, A. Tomita, *Chem. Commun.* **1997**, 701-702.
[18] B. R. Martin, D. J. Dermody, B. D. Reiss, M. Fang, L. A. Lyon, M. J. Natan, T. E. Mallouk, *Adv. Mater.* **1999**, *11*, 1021-1025.
[19] B. M. I. van der Zande, M. R. Böhmer, L. G. J. Fokkink, C. Schönenberger, *Langmuir* **2000**, *16*, 451-458.
[20] N. R. Jana, L. Gearheart, C. J. Murphy, *J. Phys. Chem. B* **2001**, *105*, 4065-4067.
[21] B. Nikoobakht, M. A. El-Sayed, *Chem. Mater.* **2003**, *15*, 1957-1962.
[22] K. Liu, N. Zhao, E. Kumacheva, *Chem. Soc. Rev.* **2011**, *40*, 656-671.
[23] L. Vigderman, E. R. Zubarev, *Chem. Mater.* **2013**, *25*, 1450-1457.
[24] B. D. Busbee, S. O. Obare, C. J. Murphy, *Adv. Mater.* **2003**, *15*, 414-416.
[25] C. J. Murphy, N. R. Jana, *Adv. Mater.* **2002**, *14*, 80-82.
[26] L. Gou, C. J. Murphy, *Chem. Mater.* **2005**, *17*, 3668-3672.
[27] C. J. Johnson, E. Dujardin, S. A. Davis, C. J. Murphy, S. Mann, *J. Mater. Chem.* **2002**, *12*, 1765-1770.
[28] N. R. Jana, L. Gearheart, C. J. Murphy, *Adv. Mater.* **2001**, *13*, 1389-1393.
[29] I. Pastoriza-Santos, J. Pérez-Juste, L. M. Liz-Marzán, *Chem. Mater.* **2006**, *18*, 2465-2467.
[30] T. K. Sau, C. J. Murphy, *Langmuir* **2004**, *20*, 6414-6420.
[31] L. M. Liz-Marzán, M. Grzelczak, *Science* **2017**, *356*, 1120-1121.
[32] A. Klinkova, E. M. Larin, E. Prince, E. H. Sargent, E. Kumacheva, *Chem. Mater.* **2016**, *28*, 3196-3202.
[33] X. Ye, L. Jin, H. Caglayan, J. Chen, G. Xing, C. Zheng, V. Doan-Nguyen, Y. Kang, N. Engheta, C. R. Kagan, C. B. Murray, *ACS Nano* **2012**, *6*, 2804-2817.
[34] X. Ye, C. Zheng, J. Chen, Y. Gao, C. B. Murray, *Nano Lett.* **2013**, *13*, 765-771.
[35] A. Liopo, S. Wang, P. J. Derry, A. A. Oraevsky, E. R. Zubarev, *RSC Adv.* **2015**, *5*, 91587-91593.
[36] N. R. Jana, L. Gearheart, C. J. Murphy, *Chem. Commun.* **2001**, 617-618.
[37] M. J. A. Hore, X. Ye, J. Ford, Y. Gao, J. Fei, Q. Wu, S. J. Rowan, R. J. Composto, C. B. Murray, B. Hammouda, *Nano Lett.* **2015**, *15*, 5730-5738.
[38] L. Zhang, K. Xia, Z. Lu, G. Li, J. Chen, Y. Deng, S. Li, F. Zhou, N. He, *Chem. Mater.* **2014**, *26*, 1794-1798.
[39] C. J. Murphy, A. M. Gole, S. E. Hunyadi, J. W. Stone, P. N. Sisco, A. Alkilany, B. E. Kinard, P. Hankins, *Chem. Commun.* **2008**, 544-557.

[40] K.-S. Lee, M. A. El-Sayed, *J. Phys. Chem. B* **2005**, *109*, 20331-20338.
[41] T. K. Sau, A. L. Rogach, *Adv. Mater.* **2010**, *22*, 1781-1804.
[42] M. Grzelczak, J. Perez-Juste, P. Mulvaney, L. M. Liz-Marzan, *Chem. Soc. Rev.* **2008**, *37*, 1783-1791.
[43] P. L. Gai, M. A. Harmer, *Nano Lett.* **2002**, *2*, 771-774.
[44] Liu, P. Guyot-Sionnest, *J. Phys. Chem. B* **2005**, *109*, 22192-22200.
[45] X. Ye, C. Zheng, J. Chen, Y. Gao, C. B. Murray, *Nano Lett.* **2013**, *13*, 765-771.
[46] X. Ye, Y. Gao, J. Chen, D. C. Reifsnyder, C. Zheng, C. B. Murray, *Nano Lett.* **2013**, *13*, 2163-2171.
[47] S. Gómez-Graña, F. Hubert, F. Testard, A. Guerrero-Martínez, I. Grillo, L. M. Liz-Marzán, O. Spalla, *Langmuir* **2012**, *28*, 1453-1459.
[48] B. Nikoobakht, M. A. El-Sayed, *Langmuir* **2001**, *17*, 6368-6374.
[49] T. K. Sau, C. J. Murphy, *Langmuir* **2005**, *21*, 2923-2929.
[50] C. J. Murphy, L. B. Thompson, A. M. Alkilany, P. N. Sisco, S. P. Boulos, S. T. Sivapalan, J. A. Yang, D. J. Chernak, J. Huang, *J. Phys. Chem. Lett.* **2010**, *1*, 2867-2875.
[51] J. Pérez-Juste, L. M. Liz-Marzán, S. Carnie, D. Y. C. Chan, P. Mulvaney, *Adv. Funct. Mater.* **2004**, *14*, 571-579.
[52] J. E. Millstone, W. Wei, M. R. Jones, H. Yoo, C. A. Mirkin, *Nano Lett.* **2008**, *8*, 2526-2529.
[53] O. M. Magnussen, *Chem. Rev.* **2002**, *102*, 679-725.
[54] J. Gao, C. M. Bender, C. J. Murphy, *Langmuir* **2003**, *19*, 9065-9070.
[55] Z. L. Wang, *J. Phys. Chem. B* **2000**, *104*, 1153-1175.
[56] C. J. Murphy, T. K. Sau, A. M. Gole, C. J. Orendorff, J. Gao, L. Gou, S. E. Hunyadi, T. Li, *J. Phys. Chem. B* **2005**, *109*, 13857-13870.
[57] S. Si, C. Leduc, M.-H. Delville, B. Lounis, *ChemPhysChem* **2012**, *13*, 193-202.
[58] C. J. Orendorff, C. J. Murphy, *J. Phys. Chem. B* **2006**, *110*, 3990-3994.
[59] M. Tebbe, C. Kuttner, M. Mayer, M. Maennel, N. Pazos-Perez, T. A. F. König, A. Fery, *J. Phys. Chem. C* **2015**, *119*, 9513-9523.
[60] B. N. Khlebtsov, Z. Liu, J. Ye, N. G. Khlebtsov, *J. Quant. Spectrosc. Radiat. Transf.* **2015**, *167*, 64-75.
[61] S. Gómez-Graña, B. Goris, T. Altantzis, C. Fernández-López, E. Carbó-Argibay, A. Guerrero-Martínez, N. Almora-Barrios, N. López, I. Pastoriza-Santos, J. Pérez-Juste, S. Bals, G. Van Tendeloo, L. M. Liz-Marzán, *J. Phys. Chem. Lett.* **2013**, *4*, 2209-2216.
[62] D. K. Smith, B. A. Korgel, *Langmuir* **2008**, *24*, 644-649.
[63] D. K. Smith, N. R. Miller, B. A. Korgel, *Langmuir* **2009**, *25*, 9518-9524.
[64] T. H. Ha, H.-J. Koo, B. H. Chung, *J. Phys. Chem. C* **2007**, *111*, 1123-1130.
[65] J. S. DuChene, W. Niu, J. M. Abendroth, Q. Sun, W. Zhao, F. Huo, W. D. Wei, *Chem. Mater.* **2013**, *25*, 1392-1399.
[66] R. G. Rayavarapu, C. Ungureanu, P. Krystek, T. G. van Leeuwen, S. Manohar, *Langmuir* **2010**, *26*, 5050-5055.
[67] N. D. Burrows, S. Harvey, F. A. Idesis, C. J. Murphy, *Langmuir* **2017**, *33*, 1891-1907.
[68] K. C. Jha, H. Liu, M. R. Bockstaller, H. Heinz, *J. Phys. Chem. C* **2013**, *117*, 25969-25981.
[69] S. K. Meena, M. Sulpizi, *Langmuir* **2013**, *29*, 14954-14961.
[70] J. Feng, R. B. Pandey, R. J. Berry, B. L. Farmer, R. R. Naik, H. Heinz, *Soft Matter* **2011**, *7*, 2113-2120.
[71] H. Ramezani-Dakhel, L. Ruan, Y. Huang, H. Heinz, *Adv. Funct. Mater.* **2015**, *25*, 1374-1384.
[72] H. Heinz, H. Ramezani-Dakhel, *Chem. Soc. Rev.* **2016**, *45*, 412-448.
[73] F. Hubert, F. Testard, O. Spalla, *Langmuir* **2008**, *24*, 9219-9222.

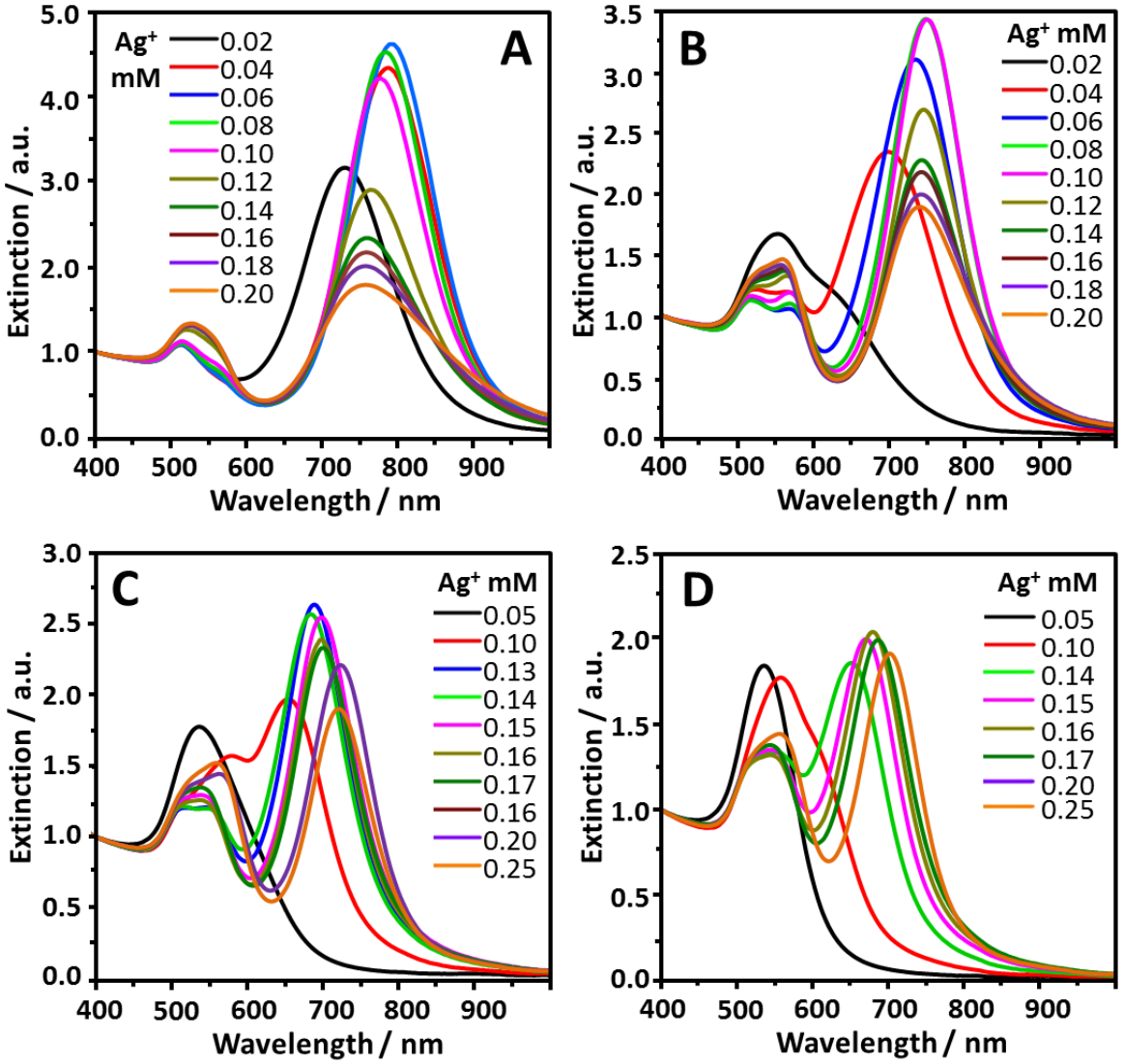

Figure 1. Extinction spectra of Au NRs prepared by the silver-assisted seed-mediated method. All parameters were kept constant (including seed type) except for the $AgNO_3$ concentrations and CTAB origin (batch and supplier). In this regard, four CTABs with different inherent iodide concentrations, ((A) 0.48, (B) 1.0, (C) 1.48, and (D) 1.99 $mgkg^{-1}$) were used.

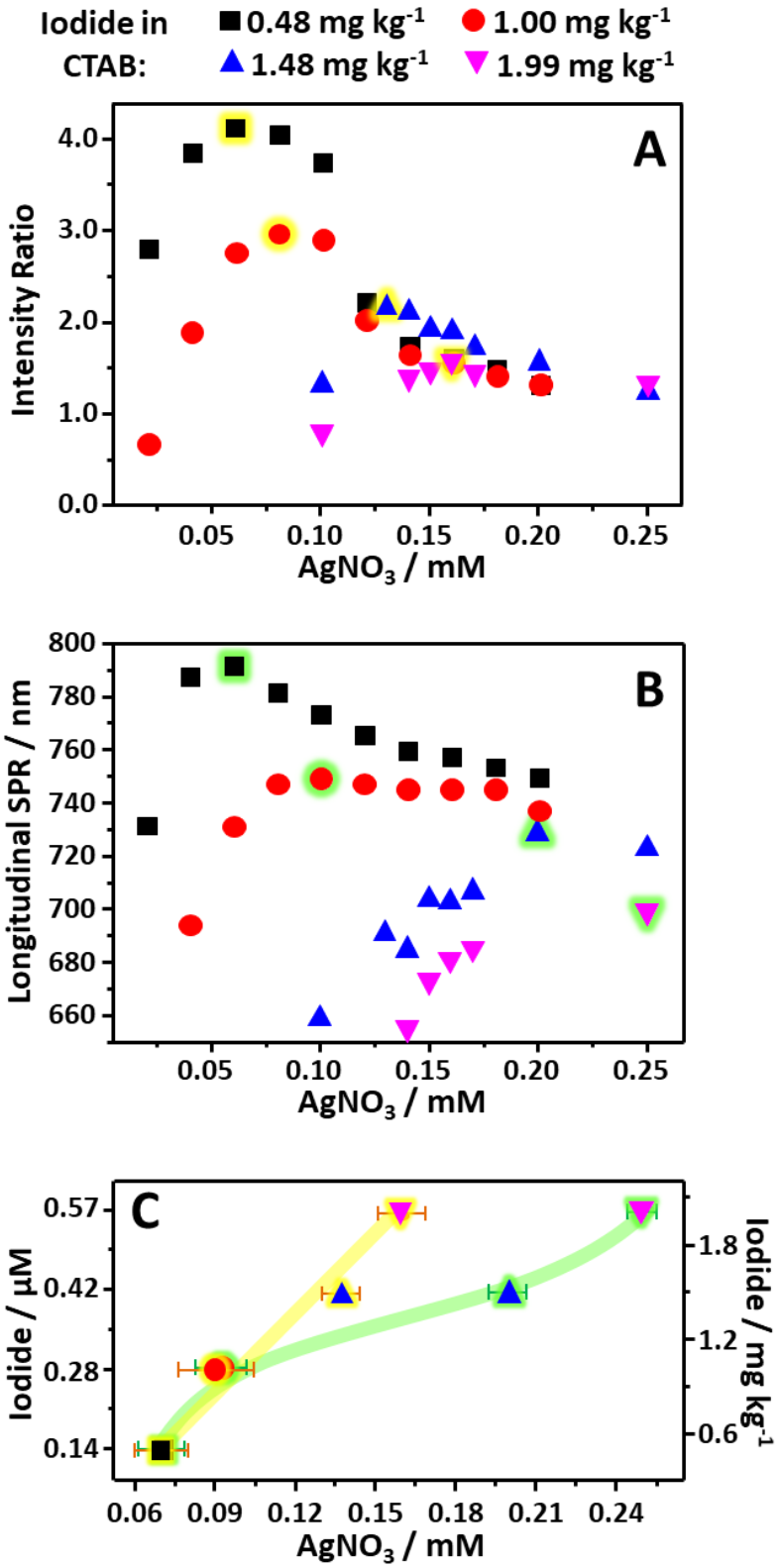

Figure 2. (A) Calculated intensity ratios between the longitudinal and the transverse peak (I_L/I_T) versus $AgNO_3$ concentration, for different iodide contents present in CTAB. (B) Longitudinal SPR peak position plotted vs. $AgNO_3$ concentration, for different iodide contents. (C) Amounts of $AgNO_3$ providing the maximum Au NR yield (highlighted in yellow) and more red-shifted longitudinal SPR (highlighted in green) for each iodide content. Note that the values in (A) and (B) were calculated from the UV-Vis spectra shown in Figure 1, whereas data in (C) are the average values for different synthesis (n=4).

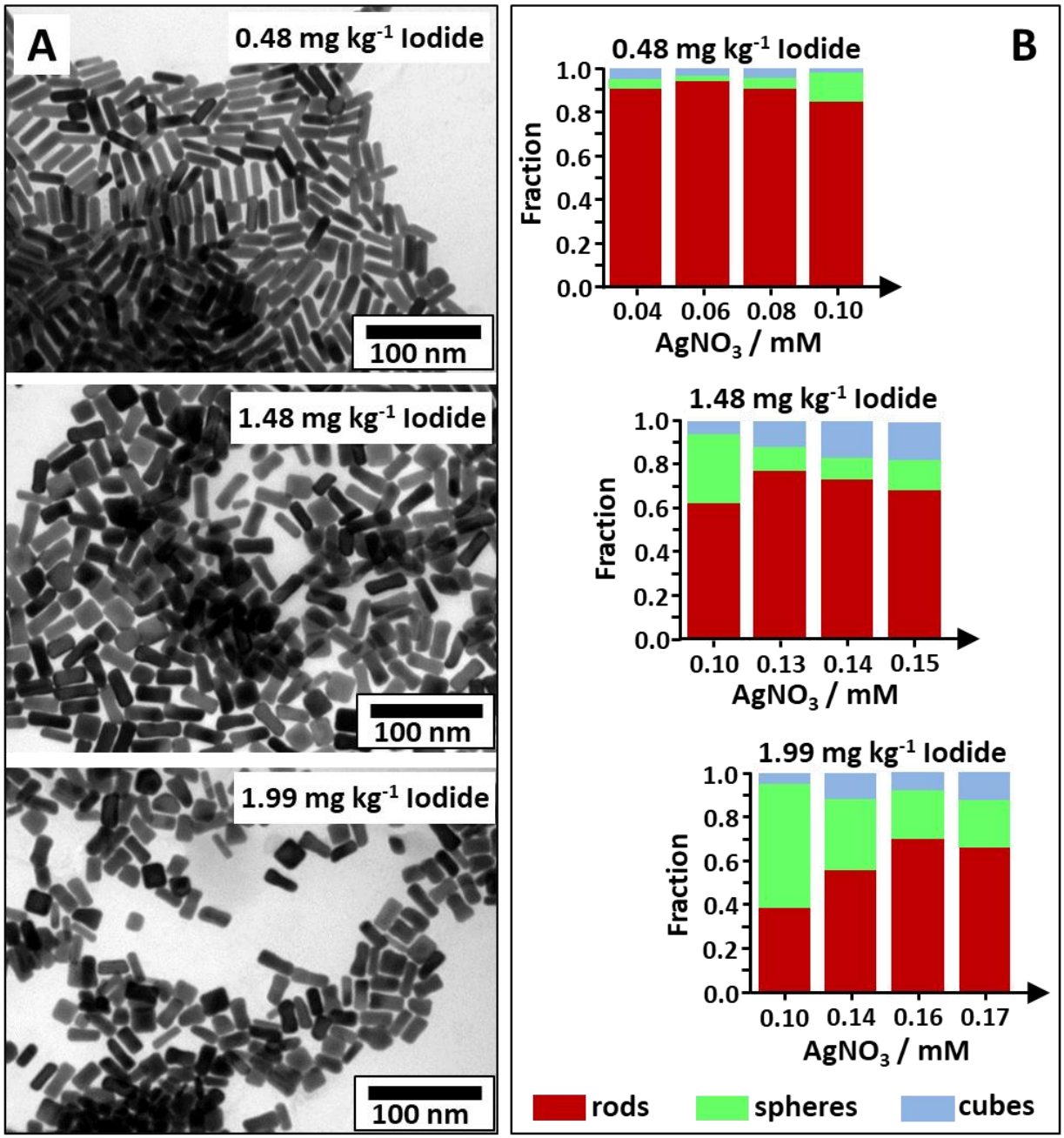

Figure 3. (A) Representative TEM images of Au NRs fabricated from growth solutions with different iodide content (0.48, 1.48 and 1.99 mg kg^{-1}) and optimized $AgNO_3$ concentration (0.06, 0.13 and 0.16 mM). (B) Morphological distribution (rods, spheres, and cubes) of nanoparticles in the colloidal dispersions for different $AgNO_3$ concentrations.

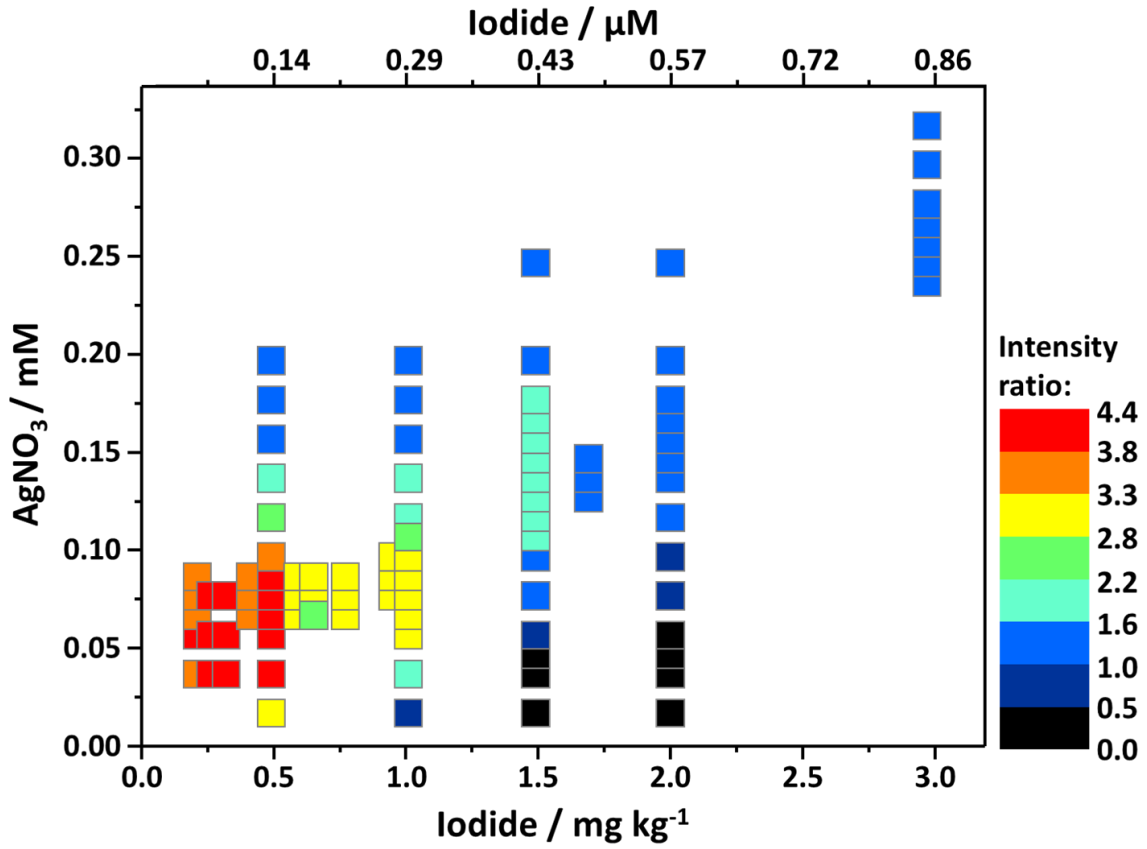

Figure 4. Intensity ratios of Au NRs colloids obtained by tuning the $AgNO_3$ concentration for different iodide contents in the CTABs and their mixtures. The color of the squares indicates the magnitude of the intensity ratio.

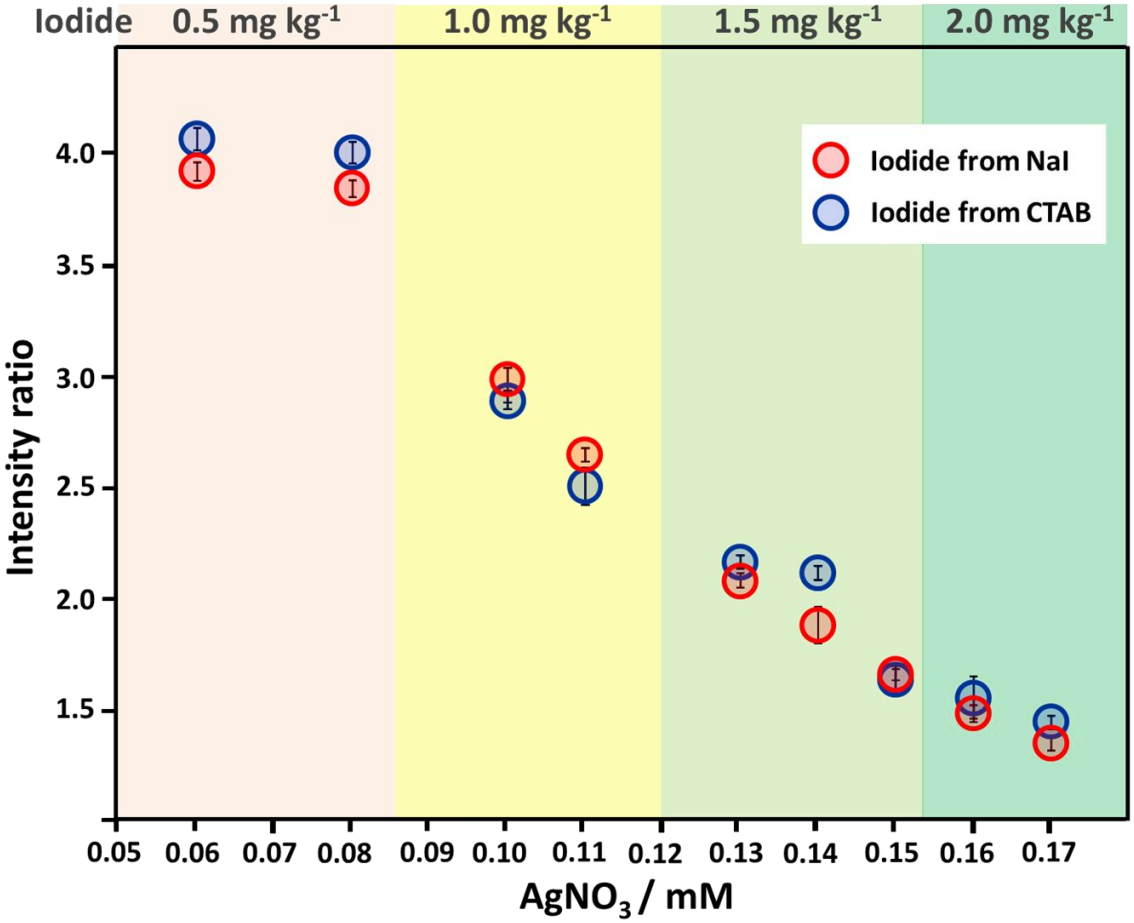

Figure 5. Intensity ratio maxima for Au NRs colloids at different iodide contents (0.5, 1.0, 1.5, and 2.0 mg kg^{-1}) against the Ag^{+} concentrations required to maximize the Au NR yield. The blue dots correspond to colloids with iodide content originating solely as an internal impurity of CTAB. The red dots are from colloidal syntheses using CTAB with the lowest iodide content and adding NaI as an external source of iodide.

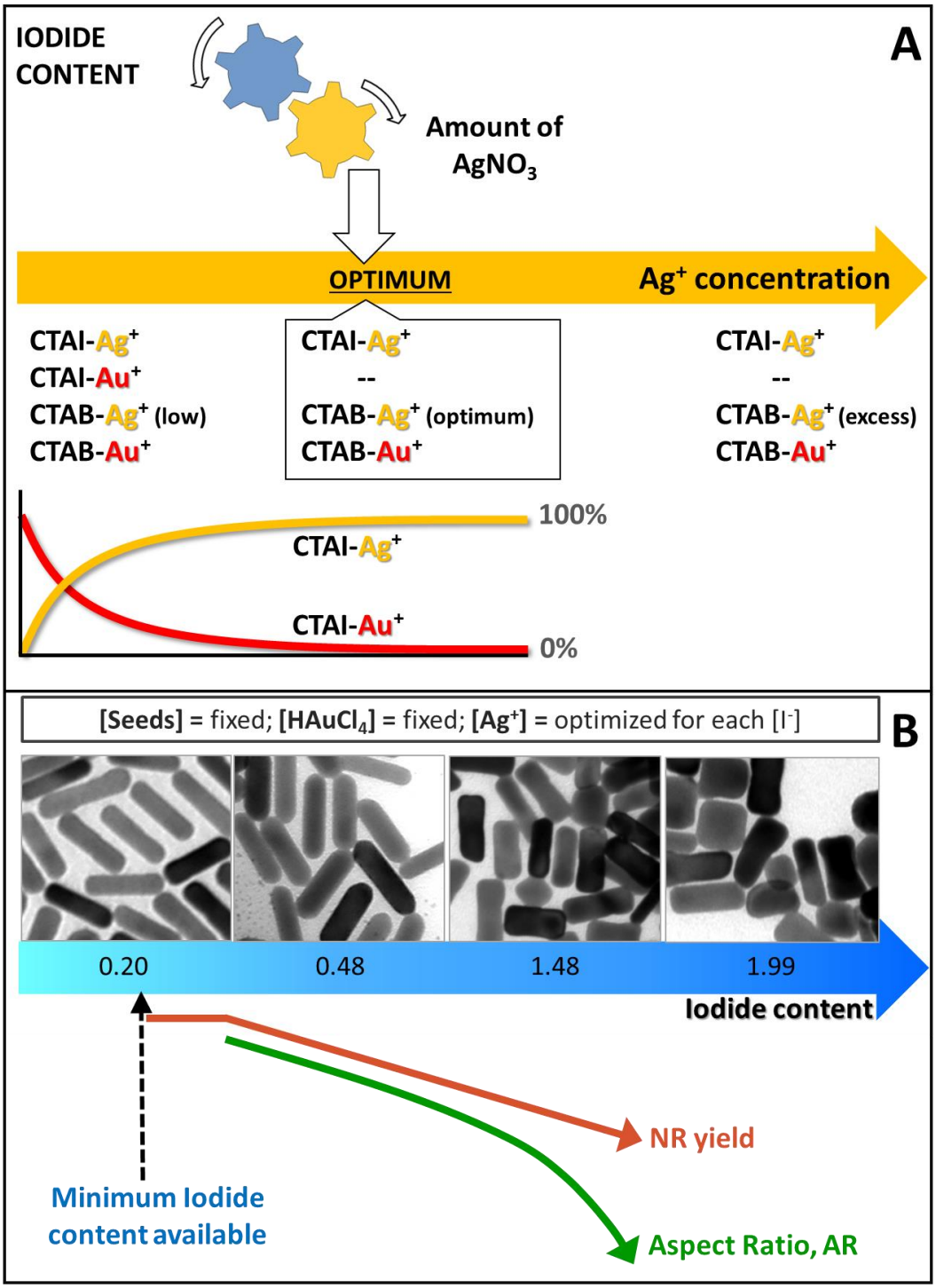

Figure 6. Schematic outline of (A) the optimal tuning of the Ag^+ concentration for a fixed iodide content, and (B) effect of iodide content on Au NR yield and morphology for fixed amount of seeds and $HAuCl_4$ concentration (Ag^+ concentration is assumed to be the optimized value for each iodide content, as depicted in (A)).

Table 1. List of CTAB reagents and corresponding suppliers, batches and iodide contents (determined by ICP-MS).

Supplier	Batch Nº	Iodide Content (mg kg^{-1})
Merck	K93365042 319	0.20
Merck	K93377642 325	0.25
Merck	K93093842 050	0.31
Merck	K93365042 319	0.40
Merck	K93258242 225	0.48
Sigma-Aldrich	091M0156V	1.00
Sigma-Aldrich	091M0156V	1.48
Sigma-Aldrich	091M0156V	1.99
Merck	K91921142 432	555

Table 2. Shows the optimized values of [Ag] to obtain the maximum yield of Au NRs (intensity ratio) for each iodide content on the investigated CTABs. This table is summary of the data plotted in **Figure 4**.

Iodide Content (mg kg^{-1})	Optimized [Ag] (mM)	Intensity Ratio (IR) Maximum	IR Deviation
0.20	0.06 ± 0.01	4.01	- 0.23
0.25	0.06 ± 0.02	4.24	- 0.02
0.31	0.06 ± 0.02	4.37	- 0.02
0.40	0.08 ± 0.01	3.65	- 0.12
0.48	0.07 ± 0.01	4.09	- 0.03
0.58	0.08 ± 0.01	3.18	- 0.09
0.64	0.08 ± 0.01	2.82	- 0.05
0.76	0.08 ± 0.01	2.97	- 0.08
0.94	0.09 ± 0.01	2.94	- 0.15
1.00	0.09 ± 0.01	2.94	- 0.03
1.48	0.13 ± 0.01	2.16	- 0.09
1.68	0.14 ± 0.01	1.63	- 0.06
1.99	0.16 ± 0.01	1.56	- 0.10
2.96	0.28 ± 0.02	1.32	- 0.07

The table of contents entry:

Unveiling the direct correlation between the (unpredictable) iodide content existing as an impurity in the CTAB reagent, and the silver amount required to maximize the fabrication of high-quality Au nanorods in high yields.

Keyword: gold nanorods

Sarah Jessl, Moritz Tebbe, Luca Guerrini, Andreas Fery,* Ramon A. Alvarez-Puebla* and Nicolas Pazos-Perez*

Silver-assisted synthesis of gold nanorods: the relation between silver additive and iodide impurities

ToC figure